Fermi Surface of Sr_2RuO_4: Spin-Orbit and Anisotropic Coulomb Interaction Effects

Guoren Zhang,[1] Evgeny Gorelov,[1] Esmaeel Sarvestani,[1] and Eva Pavarini[1,2]
[1]*Institute for Advanced Simulation, Forschungszentrum Jülich, D-52425 Jülich, Germany*
[2]*JARA High-Performance Computing, RWTH Aachen University, 52062 Aachen, Germany*
(Received 15 July 2015; published 8 March 2016)

The topology of the Fermi surface of Sr_2RuO_4 is well described by local-density approximation calculations with spin-orbit interaction, but the relative size of its different sheets is not. By accounting for many-body effects via dynamical mean-field theory, we show that the standard isotropic Coulomb interaction alone worsens or does not correct this discrepancy. In order to reproduce experiments, it is essential to account for the Coulomb anisotropy. The latter is small but has strong effects; it competes with the Coulomb-enhanced spin-orbit coupling and the isotropic Coulomb term in determining the Fermi surface shape. Its effects are likely sizable in other correlated multiorbital systems. In addition, we find that the low-energy self-energy matrix—responsible for the reshaping of the Fermi surface—sizably differs from the static Hartree-Fock limit. Finally, we find a strong spin-orbital entanglement; this supports the view that the conventional description of Cooper pairs via factorized spin and orbital part might not apply to Sr_2RuO_4.

DOI: 10.1103/PhysRevLett.116.106402

Sr_2RuO_4 has attracted a lot of attention as a possible realization of a spin-triplet superconductor [1–4] and, at the same time, as a very peculiar strongly correlated metal [5–13]. Understanding the details of its Fermi surface (FS) is key to unraveling the nature of quasielectrons in the normal phase and can cast light on the mechanism and the symmetry of the superconducting order parameter. It is thus not surprising that the Fermi surface of Sr_2RuO_4 has been intensively investigated, both experimentally [14–20] and theoretically [21–23]. Although the main features are nowadays well understood, the effects of the interplay between correlations, spin-orbit, and crystal structure have not been fully disentangled yet.

Sr_2RuO_4 is a tetragonal layered perovskite (space group $I4/mmm$ [24]) with the Ru $4d^4$ ($t_{2g}^4 e_g^0$) electronic configuration and Ru atoms at sites with D_{4h} symmetry; due to the layered structure the Ru t_{2g}, xz and yz bands are almost one dimensional and very narrow, with a bandwidth $W_{xz} = W_{yz}$ about half as large as that of the two-dimensional Ru xy band, W_{xy}. Experimentally, the Fermi surface of Sr_2RuO_4 has been studied via both the de Haas–van Alphen technique [14–16] and angle-resolved photoemission spectroscopy (ARPES) [17–20]. It is made (Fig. 1) by three sheets, the electronlike γ (xy band) and β (xz, yz bands) sheets and the holelike α sheet (xz, yz bands). Theoretically, *ab initio* calculations based on the local-density approximation (LDA) qualitatively reproduce the FS topology, provided that the spin-orbit (SO) interaction is taken into account [22,23]. Indeed, several experiments point to a sizable SO coupling [1,25,26]. These calculations fail, however, in describing the relative size of the sheets, suggesting that perhaps many-body effects play a key role. The relevance of the Coulomb interaction for the electronic properties of Sr_2RuO_4, as well as its interplay with bands of different width, was shown early on via model many-body studies [21]. More recently, LDA+DMFT (local-density approximation + dynamical mean-field theory) calculations have emphasized the interplay of Coulomb

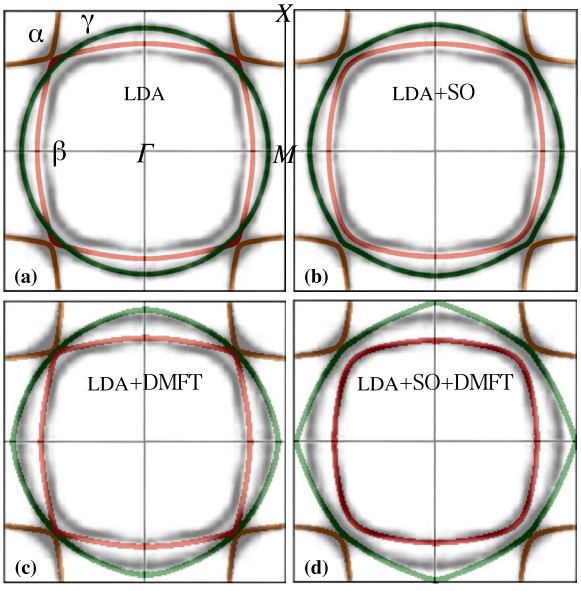

FIG. 1. Fermi surface ($k_z = 0$) of Sr_2RuO_4 from (a) LDA, (b) LDA + SO, (c) LDA + DMFT, and (d) LDA + SO + DMFT calculations performed with $O(3)$-symmetric Coulomb matrix, $(U, J) = (3.1, 0.7)$ eV, $T \to 0$ limit. (Light lines) α and β sheets. (Dark lines) γ sheet. (Gray density maps) Experimental data taken from Ref. [17].

interaction and t_{2g} crystal field (CF) [9,27], and the role of the Hund's rule coupling [10]. LDA + slave-boson calculations point to SO effects on the correlated bands [28]. It remains, however, unclear to what extent many-body effects actually modify the Fermi surface, and how they compete with other effects.

In this Letter, by using the LDA + DMFT method with SO interaction, we investigate, for the first time, the interplay between Coulomb repulsion, spin-orbit, and symmetry at the Fermi surface in a realistic setting. We show that, surprisingly, the standard isotropic Coulomb interaction alone [$O(3)$ symmetry] does not improve (or even worsens) the agreement between theoretical and experimental Fermi surface. The agreement with experiments can be achieved only if both SO and Ru D_{4h} low-symmetry Coulomb terms are taken into account. These terms are often neglected in realistic many-body calculations due to the numerical difficulties of treating them. In order to efficiently deal with many-body Hamiltonians of arbitrary symmetry we have recently developed a generalized LDA + DMFT solver [9,29,30] based on the continuous-time (CT) quantum Monte Carlo (QMC) [31] technique. Here, we use the interaction-expansion [32] flavor (CT-INT) of this solver [9], further extended to account for SO terms. We show that, remarkably, D_{4h} low-symmetry Coulomb terms compete with the standard isotropic $O(3)$ terms, the crystal field, and the SO coupling in determining the actual shape of the FS of Sr_2RuO_4.

In the first step we perform LDA calculations using the full-potential linearized augmented plane-wave method (WIEN2K [33] code), with and without SO interaction. Next we construct localized t_{2g} Wannier functions via Marzari-Vanderbilt localization [34,35] and t_{2g} projectors [36]. Finally, we build the t_{2g} Hubbard model

$$H = -\sum_{jj'}\sum_{\sigma\sigma'}\sum_{mm'} t^{j,j'}_{m\sigma,m'\sigma'} c^{\dagger}_{jm\sigma} c_{j'm'\sigma'} + \frac{1}{2}\sum_{j}\sum_{\sigma\sigma'}\sum_{mm'pp'} U_{mm'pp'} c^{\dagger}_{jm\sigma} c^{\dagger}_{jm'\sigma'} c_{jp'\sigma'} c_{jp\sigma} - H_{\mathrm{dc}}. \quad (1)$$

Here, $c^{\dagger}_{jm\sigma}$ ($c_{jm\sigma}$) creates (destroys) an electron with spin σ in the Wannier state with orbital quantum number m ($m = xy, yz, xz$) at site j; H_{dc} is the double-counting correction [37]; $-t^{j,j'}_{m\sigma,m'\sigma'}$ are the hopping integrals ($j \neq j'$) and the elements of the on-site energy matrix ($j = j'$). The latter includes crystal field splittings and, when present, the SO term $\mathbf{l}\cdot\underline{\lambda}\cdot\mathbf{s}$, where $\underline{\lambda}$ is the coupling constant tensor. After ordering the states as $\{|m\rangle_{\uparrow}\}, \{|m\rangle_{\downarrow}\}$, the on-site matrix $\varepsilon_{m\sigma,m'\sigma'} = -t^{j,j}_{m\sigma,m'\sigma'}$ takes the form

$$\hat{\varepsilon} = \begin{pmatrix} \varepsilon_{xy} & 0 & 0 & 0 & \frac{\lambda_{xy}}{2} & \frac{i\lambda_{xy}}{2} \\ 0 & \varepsilon_{yz} & -\frac{i\lambda_z}{2} & -\frac{\lambda_{xy}}{2} & 0 & 0 \\ 0 & \frac{i\lambda_z}{2} & \varepsilon_{xz} & -\frac{i\lambda_{xy}}{2} & 0 & 0 \\ 0 & -\frac{\lambda_{xy}}{2} & \frac{i\lambda_{xy}}{2} & \varepsilon_{xy} & 0 & 0 \\ \frac{\lambda_{xy}}{2} & 0 & 0 & 0 & \varepsilon_{yz} & \frac{i\lambda_z}{2} \\ -\frac{i\lambda_{xy}}{2} & 0 & 0 & 0 & -\frac{i\lambda_z}{2} & \varepsilon_{xz} \end{pmatrix}.$$

Because of D_{4h} site symmetry, the Ru t_{2g} states split into an e_g doublet (xz, yz) and a b_{2g} singlet (xy), with on-site energy $\varepsilon_{xz} = \varepsilon_{yz}$ and ε_{xy}, respectively. LDA yields $\varepsilon_{xz} = \varepsilon_{xy} + \varepsilon_{\mathrm{CF}}$ with $\varepsilon_{\mathrm{CF}} \sim 120$ meV. The SO parameter λ_z couples the orbital $|yz\rangle_{\sigma}$ to the orbital $|xz\rangle_{\sigma}$; instead, the term λ_{xy} couples the $|xy\rangle_{\sigma}$ state to the $|yz\rangle_{-\sigma}$ and $|xz\rangle_{-\sigma}$ orbitals. LDA yields $\lambda_z \sim 102$ meV and $\lambda_{xy} \sim 100$ meV, i.e., 15% smaller than the value 130 ± 30 meV estimated via spin-resolved photoemission spectroscopy [26]. The LDA tetragonal anisotropy $\delta_{\lambda} = \lambda_z - \lambda_{xy}$, is tiny, $\delta_{\lambda} \sim 2$ meV. The terms $U_{mm'pp'}$ are elements of the screened Coulomb interaction tensor. For a free atom the Coulomb interaction tensor for d states can be written in terms of the three Slater integrals F_0, F_2, and F_4. For t_{2g} states the essential terms [38] are the direct $[U_{mm'mm'} = U_{m,m'} = U - 2J(1-\delta_{m,m'})]$ and the exchange ($U_{mm'm'm} = J$) screened Coulomb interaction, the pair-hopping ($U_{mmm'm'} = J$) and the spin-flip term ($U_{mm'm'm} = J$); here $U = F_0 + \frac{4}{49}(F_2 + F_4)$ and $J = \frac{1}{49}(3F_2 + \frac{20}{9}F_4)$. For site symmetry D_{4h} the number of independent Coulomb parameters increases to six. Here we will discuss, in particular, the effect of $\Delta U = U_{xy,xy} - U_{xz,xz}$ and $\Delta U' = U_{xy,yz} - U_{xz,yz}$. We solve (1) with DMFT using the CT-INT QMC method. We work with a 6×6 self-energy matrix $\Sigma_{m\sigma,m'\sigma'}(\omega) = \Sigma'_{m\sigma,m'\sigma'}(\omega) + i\Sigma''_{m\sigma,m'\sigma'}(\omega)$ in spin-orbital space, extending the solver of Ref. [9] to deal explicitly with the SO term; Σ' is the real and Σ'' the imaginary part of the self-energy. The calculations with SO coupling are performed in the basis $|\tilde{m}\rangle_{\sigma} = \hat{T}|m\rangle_{\sigma}$, where the unitary operator $\hat{T}$ is chosen such that the local imaginary-time Green function matrix is real. In the rest of the Letter, for calculations with SO coupling, the elements of the self-energy matrix are given in the $|\tilde{m}\rangle_{\sigma}$ basis; since $\hat{T}$ only changes the phases [39] but does not mix orbitals, we rename for simplicity $|\tilde{m}\rangle_{\sigma}$ as $|m\rangle_{\sigma}$.

First, let us analyze the LDA results without SO interaction [Fig. 1(a)]. Our results agree very well with previous theoretical works [22,23,40,41]. Compared with ARPES data, LDA describes well the α and γ sheets, and in particular the region around the M point of the γ sheet. There are two major discrepancies. First, the LDA β and γ sheets cross, differently than in ARPES. Second, the area enclosed by the β sheet is larger in LDA than in ARPES.

Once the SO interaction is switched on three relevant changes occur, as Fig. 1(b) shows. The $\beta-\gamma$ crossing becomes an anticrossing due to the SO coupling λ_{xy}; the β sheet shrinks and the γ sheet expands. These effects improve the overall agreement [22,23,26] with ARPES results; however, the β sheet remains too large with respect to experiments.

The next step consists in incorporating the Coulomb interaction via LDA + DMFT [see Fig. 1(c)]. First, we perform standard calculations with no SO term and $O(3)$-symmetric Coulomb tensor. We use two sets of parameters: $(U,J)=(3.1,0.7)$ eV, as obtained via constrained LDA [42], and $(U,J)=(2.3,0.4)$ eV, as obtained via constrained random-phase approximation [43] (CRPA). These sets of values yield spectral functions with Hubbard bands in line with available experiments [7,42,44,45]. Low-energy many-body effects change the splitting $\varepsilon_{\rm CF}$ into $\varepsilon_{\rm CF}+\Delta\varepsilon_{\rm CF}$, with [46]

$$\Delta\varepsilon_{\rm CF}=\frac{1}{2}\Sigma'_{yz\sigma,yz\sigma}(0)+\frac{1}{2}\Sigma'_{xz\sigma,xz\sigma}(0)-\Sigma'_{xy\sigma,xy\sigma}(0).$$

The shift $\Delta\varepsilon_{\rm CF}$ turns out to be positive [21]; at $T=290$ K we find $\Delta\varepsilon_{\rm CF}=108$ meV for $(U,J)=(3.1,0.7)$ eV and 80 meV for $(U,J)=(2.3,0.4)$ eV. As a consequence, with respect to LDA, the α and γ sheets expand whereas the β sheet shrinks. This is shown in Fig. 1(c) for $(U,J)=(3.1,0.7)$ eV; the LDA + DMFT Fermi surface deviates from ARPES in particular around the M point (γ sheet), which approaches the boundary of the first Brillouin zone. For $(U,J)=(2.3,0.4)$ eV the effect is smaller and the FS remains closer to the LDA one [47].

In Fig. 1(d) we show the effect of including the SO term (LDA + SO + DMFT). We find a $\Delta\varepsilon_{\rm CF}$ slightly smaller than for $\lambda_i=0$; the SO couplings are, however, sizably enhanced with respect to LDA, i.e., $\lambda_i\to\lambda_i+\Delta\lambda_i$, with

$$\Delta\lambda_z=-[\Sigma'_{yz\uparrow,xz\uparrow}(0)+\Sigma'_{yz\downarrow,xz\downarrow}(0)],$$
$$\Delta\lambda_{xy}=\frac{1}{2}\sum_\sigma\sigma[\Sigma'_{xy\sigma,yz-\sigma}(0)-\Sigma'_{xy\sigma,xz-\sigma}(0)].$$

At 290 K we obtain $\Delta\lambda_{xy}\sim 96$ meV and $\Delta\lambda_z\sim 88$ meV. For the FS, with respect to LDA + DMFT, the agreement worsens for the γ sheet and it improves for the α and β sheets. The change can be ascribed to the enhanced SO couplings. Comparing Figs. 1(b) and 1(c) with Fig. 1(d) it appears that the combined effect of Coulomb and SO interaction results in the γ sheet approaching the boundary of the first Brillouin zone. For $(U,J)=(2.3,0.4)$ eV the effects of the SO coupling are qualitatively similar [47]. These results point to the existence of an important mechanism neglected so far.

We identify the missing mechanism in low-symmetry Coulomb terms. Because of the elongation of the RuO bond in the **c** direction, the e_g (xz,yz) Wannier orbitals have a larger spread than xy orbital [48], suggesting positive ΔU and $\Delta U'$. This is in line with the results of CRPA, $\Delta U\sim 0.3$ eV [43]. To study the effect of the Coulomb anisotropy we perform two additional sets of LDA + SO + DMFT calculations, the first with $0<\Delta U<0.6$ eV and $\Delta U'=0$ and the second with $0<\Delta U'=\Delta U/3<0.2$ eV [49]. The most significant results are shown in Fig. 2 for $T=290$ K [50]. We find that both $\Delta\lambda_z$ and $\Delta\lambda_{xy}$ are weakly dependent on ΔU. Instead, $\Delta\varepsilon_{\rm CF}$ decreases linearly with ΔU and changes sign at a quite small $\Delta U\sim 0.25$ eV; at this value the effective CF has the LDA value [51]. As a consequence, the area enclosed by the γ sheet decreases as well. In Fig. 3 we present the same quantities shown in Fig. 2, however, as a function of the temperature T; we find that the tetragonal SO splitting $|\Delta\delta_\lambda|$ increases on lowering T, while $|\Delta\varepsilon_{\rm CF}|$ decreases slightly. In comparison with the strong dependence of $\Delta\varepsilon_{\rm CF}$ with ΔU, all parameters change weakly on lowering T [52].

Remarkably, these effects are to a large extent dynamical in nature [47,53]. The zero-frequency crystal-field enhancement is given by $\Delta\varepsilon_{\rm CF}=\Delta\Sigma'(\infty)+(1/\pi)\int d\omega\Delta\Sigma''(\omega)/\omega$. The term $\Delta\Sigma'(\infty)$ can be obtained via the static mean-field Hartree-Fock method; in the $\Delta U=\Delta U'=0$ case one can show that $\Delta\Sigma'(\infty)\sim\frac{1}{2}(U-5J)p$, where $p=n_{xy}-\frac{1}{2}(n_{xz}+n_{yz})$ is the orbital polarization. Because of the bandwidth mismatch [9] the LDA total polarization is $p\sim -0.17$, i.e., negative, despite of the positive CF splitting; in LDA + DMFT it becomes basically zero, hence $\Delta\Sigma'(\infty)\sim 0$ as well. The enhancement $\Delta\varepsilon_{\rm CF}>0$ comes thus essentially from the second term; it turns out, by analyzing the integrand $\Delta\Sigma''(\omega)/\omega$, that it has large contributions from the lower Hubbard bands. The SO interaction

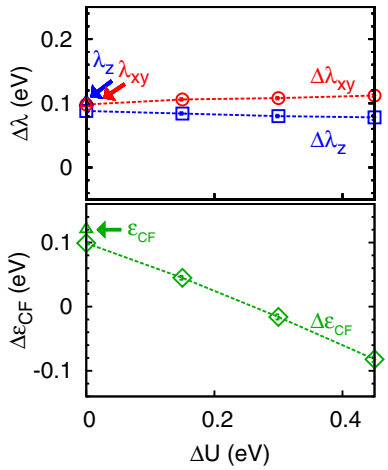

FIG. 2. Many-body corrections of the on-site parameters at the Fermi energy as a function of ΔU, with $\Delta U'=\Delta U/3$. The LDA + SO + DMFT calculations are done at $T=290$ K and for $(U,J)=(3.1,0.7)$ eV. (Top) Spin-orbit couplings corrections, $\Delta\lambda_z$ and $\Delta\lambda_{xy}$. (Bottom) Crystal-field splitting correction, $\Delta\varepsilon_{\rm CF}$. The LDA values λ_z, λ_{xy}, and $\varepsilon_{\rm CF}$ are indicated by arrows. QMC error bars are shown.

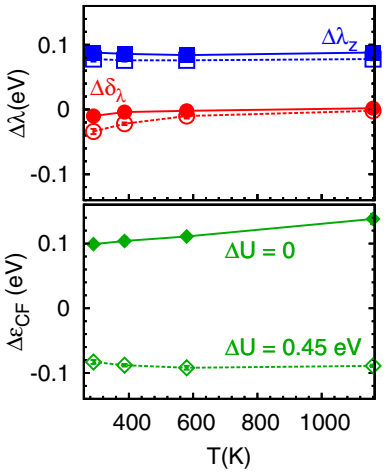

FIG. 3. Many-body corrections of the on-site parameters at the Fermi energy as a function of temperature and for $(U, J) = (3.1, 0.7)$ eV. (Top) Spin-orbit coupling corrections, $\Delta\lambda_z$ and $\Delta\delta_\lambda = \Delta\lambda_z - \Delta\lambda_{xy}$. (Bottom) Crystal-field splitting correction $\Delta\varepsilon_{\mathrm{CF}}$. (Solid lines) $\Delta U = 0$. (Dashed lines) $\Delta U = 0.45$ eV. All calculations are performed for $\Delta U' = \Delta U/3$. QMC error bars are shown.

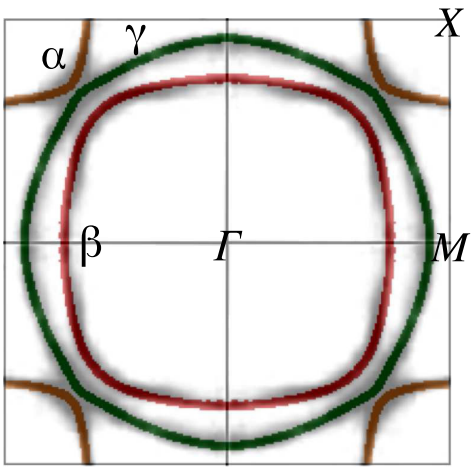

FIG. 4. Fermi surface ($k_z = 0$) of Sr_2RuO_4 from LDA + SO + DMFT calculations with D_{4h} Coulomb terms and $(U,J) = (3.1,0.7)$ eV, $T \to 0$ limit. (Parameters) $\Delta\varepsilon_{\mathrm{CF}} \sim -0.02$ eV, $\Delta\lambda_{xy} \sim 0.13$ eV, $\Delta\lambda_z \sim 0.08$ eV, values approximatively corresponding to $\Delta U = 3\Delta U' = 0.3$ eV. (Gray density maps) Experimental data from Ref. [17].

does not affect much the CF splitting, but it slightly increases the initial orbital polarization, from $p = -0.17$ (LDA) to $p = -0.19$ (LDA + SO); furthermore, it couples the e_g and b_{2g} orbitals, yielding a negative SO polarization $p_j \sim -0.10$, with $p_j \equiv n_{3/2} - n_{1/2}$, where n_j is the average occupation of an orbital with total angular momentum j; switching on the Coulomb interaction reduces the orbital polarization $p \sim 0$ and slightly increases $p_j \sim -0.12$. Finally, when $\Delta U > 0$, electrons are transferred from the xy to the xz and yz bands as $\Delta\varepsilon_{\mathrm{CF}}$ decreases, yielding a negative orbital polarization $p \sim -0.11$ for $\Delta U = 0.45$ eV [54].

Returning to the FS, we find that the agreement between calculations and experiments can only be recovered if both low-symmetry Coulomb terms and correlation-enhanced SO couplings are included in the calculations. To show this and test the robustness of our conclusion, in addition to LDA + SO + DMFT calculations for $\Delta U = 0.3$ eV (CRPA estimate) we perform a series of model calculations. For the latter we take $\Delta\varepsilon_{\mathrm{CF}}$ in the interval $[-0.08, -0.02]$ eV, $\Delta\lambda_{xy}$ and $\Delta\lambda_z$ in the intervals [0.10,0.16] eV and [0.04,0.08] eV [55]. These intervals estimate the possible input parameters variations and are chosen around the results in Fig. 2 for $0.3\ \mathrm{eV} \leq \Delta U \leq 0.45$ eV. In this realistic parameter range the theoretical FS is in very good agreement with experiments [56], as shown in a representative case in Fig. 4.

Our results have consequences concerning the nature of Cooper pairs. It is often assumed that Cooper pairs can be classified as singlets or triplets [1,3,4]. Recently, it was pointed out that in Sr_2RuO_4 this scenario might break down due to the SO interaction [26]. Indeed, already in LDA the SO coupling is comparable with the crystal-field splitting. Turning on the Coulomb interaction, for $\Delta U > 0$ we find that the ratio $(\lambda_i + \Delta\lambda_i)/|\varepsilon_{\mathrm{CF}} + \Delta\varepsilon_{\mathrm{CF}}|$ becomes even larger than $\lambda_i/\varepsilon_{\mathrm{CF}}$. This points to a strong spin-orbital entanglement, which should not be neglected in studying the nature of Cooper pairs, as suggested in Refs. [26,57].

In conclusion, we investigate in a realistic setting how different mechanisms affect the topology of the Fermi surface of Sr_2RuO_4. LDA calculations with spin-orbit effects describe well the topology of the Fermi surface, but not the relative size of the Fermi sheets. We show that adding alone the effects of the standard isotropic Coulomb interaction via dynamical mean-field theory does not improve (or even worsens) the agreement with experiments. It is essential to also include the small anisotropic part of the Coulomb interaction. Remarkably, we find that (small) low-symmetry Coulomb terms have a large effect at the Fermi surface. The standard isotropic Coulomb interaction enhances the crystal-field splitting and the spin-orbit coupling. The Coulomb-enhanced spin-orbit coupling shrinks the β sheet and extents the γ sheet. The low-symmetry Coulomb term ΔU reduces the Coulomb crystal-field enhancement, modifying correspondingly the α and γ sheets. To reproduce the experimental Fermi surface all these interactions are essential. Our results support the recent suggestions of strong spin-orbital entanglement for Cooper pairs. These mechanisms could be at work also in other multiorbital correlated systems: other layered metallic ruthenates, iridates, or iron-based superconductors.

We acknowledge financial support from the Deutsche Forschungsgemeinschaft through research unit FOR1346. The calculations were done on the Jülich Blue Gene/Q.

[1] T. M. Rice and M. Sigrist, J. Phys. Condens. Matter **7**, L643 (1995).
[2] K. Ishida, H. Mukuda, Y. Kitaoka, K. Asayama, Z. Q. Mao, Y. Mori, and Y. Maeno, Nature (London) **396**, 658 (1998).
[3] A. P. Mackenzie and Y. Maeno, Rev. Mod. Phys. **75**, 657 (2003).
[4] Y. Maeno, S. Kittaka, T. Nomura, S. Yonezawa, and K. Ishida, J. Phys. Soc. Jpn. **81**, 011009 (2012).
[5] C. Bergemann, A. P. Mackenzie, S. R. Julian, D. Forsythe, and E. Ohmichi, Adv. Phys. **52**, 639 (2003).
[6] N. J. C. Ingle *et al.*, Phys. Rev. B **72**, 205114 (2005).
[7] M. Schmidt, T. R. Cummins, M. Bürk, D. H. Lu, N. Nücker, S. Schuppler, and F. Lichtenberg, Phys. Rev. B **53**, R14761 (R) (1996).
[8] S. Nakatsuji and Y. Maeno, Phys. Rev. Lett. **84**, 2666 (2000).
[9] E. Gorelov, M. Karolak, T. O. Wehling, F. Lechermann, A. I. Lichtenstein, and E. Pavarini, Phys. Rev. Lett. **104**, 226401 (2010).
[10] L. de' Medici, J. Mravlje, and A. Georges, Phys. Rev. Lett. **107**, 256401 (2011).
[11] M. Malvestuto, E. Carleschi, R. Fittipaldi, E. Gorelov, E. Pavarini, M. Cuoco, Y. Maeno, F. Parmigiani, and A. Vecchione, Phys. Rev. B **83**, 165121 (2011).
[12] M. Malvestuto *et al.*, Phys. Rev. B **88**, 195143 (2013).
[13] D. Stricker, J. Mravlje, C. Berthod, R. Fittipaldi, A. Vecchione, A. Georges, and D. van der Marel, Phys. Rev. Lett. **113**, 087404 (2014).
[14] A. P. Mackenzie, S. R. Julian, A. J. Diver, G. J. McMullan, M. P. Ray, G. G. Lonzarich, Y. Maeno, S. Nishizaki, and T. Fujita, Phys. Rev. Lett. **76**, 3786 (1996).
[15] A. P. Mackenzie, S.-i. Ikeda, Y. Maeno, T. Fujita, S. R. Julian, and G. G. Lonzarich, J. Phys. Soc. Jpn. **67**, 385 (1998).
[16] A. P. Mackenzie, S. R. Julian, G. G. Lonzarich, Y. Maeno, and T. Fujita, Phys. Rev. Lett. **78**, 2271 (1997).
[17] A. Damascelli *et al.*, Phys. Rev. Lett. **85**, 5194 (2000).
[18] D. H. Lu, M. Schmidt, T. R. Cummins, S. Schuppler, F. Lichtenberg, and J. G. Bednorz, Phys. Rev. Lett. **76**, 4845 (1996).
[19] H. Iwasawa, Y. Yoshida, I. Hase, S. Koikegami, H. Hayashi, J. Jiang, K. Shimada, H. Namatame, M. Taniguchi, and Y. Aiura, Phys. Rev. Lett. **105**, 226406 (2010).
[20] S. Liu *et al.*, Phys. Rev. B **86**, 165112 (2012).
[21] A. Liebsch and A. Lichtenstein, Phys. Rev. Lett. **84**, 1591 (2000).
[22] E. Pavarini and I. I. Mazin, Phys. Rev. B **74**, 035115 (2006).
[23] M. W. Haverkort, I. S. Elfimov, L. H. Tjeng, G. A. Sawatzky, and A. Damascelli, Phys. Rev. Lett. **101**, 026406 (2008).
[24] T. Vogt and D. J. Buttrey, Phys. Rev. B **52**, R9843(R) (1995).
[25] E. J. Rozbicki, J. F. Annett, J.-R. Souquet, and A. P. Mackenzie, J. Phys. Condens. Matter **23**, 094201 (2011).
[26] C. N. Veenstra *et al.*, Phys. Rev. Lett. **112**, 127002 (2014).
[27] A. Liebsch and H. Ishida, Phys. Rev. Lett. **98**, 216403 (2007).
[28] M. Behrmann, C. Piefke, and F. Lechermann, Phys. Rev. B **86**, 045130 (2012).
[29] A. Flesch, E. Gorelov, E. Koch, and E. Pavarini, Phys. Rev. B **87**, 195141 (2013).
[30] G. Zhang, E. Gorelov, E. Koch, and E. Pavarini, Phys. Rev. B **86**, 184413 (2012).
[31] E. Gull, A. J. Millis, A. I. Lichtenstein, A. N. Rubtsov, M. Troyer, and P. Werner, Rev. Mod. Phys. **83**, 349 (2011).
[32] A. N. Rubtsov, V. V. Savkin, and A. I. Lichtenstein, Phys. Rev. B **72**, 035122 (2005).
[33] P. Blaha *et al.*, WIEN2K, *An Augmented Plane Wave+Local Orbitals Program for Calculating Crystal Properties* (Technische Universit¬at Wien, Austria, 2001).
[34] N. Marzari and D. Vanderbilt, Phys. Rev. B **56**, 12847 (1997).
[35] For the WANNIER90 code, see A. A. Mostofi, J. R. Yates, Y.-S. Lee, I. Souza, D. Vanderbilt, and N. Marzari, Comput. Phys. Commun. **178**, 685 (2008). For the interface to WIEN2K, see J. Kunes, R. Arita, P. Wissgott, A. Toschi, H. Ikeda, and K. Held, *ibid.* **181**, 1888 (2010).
[36] Projectors select Wannier functions of t_{2g} symmetry. A similar procedure is used in R. Sakuma, Phys. Rev. B **87**, 235109 (2013). Since the occupied O p states have been integrated out, the t_{2g} Wannier functions have p tails of the proper symmetry on the neighboring O sites.
[37] For $H_{\rm dc}$ we adopt an around mean-field-like form, a typical choice for correlated metals.
[38] See, e.g., E. Pavarini, in *The LDA+DMFT approach to strongly correlated materials*, edited by E. Pavarini, E. Koch, D. Vollhardt, and A. Lichtenstein, Modeling and Simulation, Vol. 1 (Forschungszentrum Jülich, Jülich, 2011), ISBN 978-3-89336-734-4, http://www.cond-mat.de/events/correl11/manuscripts/pavarini.pdf.
[39] For Sr_2RuO_4 the transformation merely amounts to an extra $(-1)^{\sigma}\pi$ phase for the $|xz\rangle_{\sigma}$ orbital.
[40] T. Oguchi, Phys. Rev. B **51**, 1385 (1995).
[41] D. J. Singh, Phys. Rev. B **52**, 1358 (1995).
[42] Z. V. Pchelkina, I. A. Nekrasov, T. Pruschke, A. Sekiyama, S. Suga, V. I. Anisimov, and D. Vollhardt, Phys. Rev. B **75**, 035122 (2007).
[43] J. Mravlje, M. Aichhorn, T. Miyake, K. Haule, G. Kotliar, and A. Georges, Phys. Rev. Lett. **106**, 096401 (2011).
[44] T. Yokoya, A. Chainani, T. Takahashi, H. Katayama-Yoshida, M. Kasai, Y. Tokura, N. Shanthi, and D. D. Sarma, Phys. Rev. B **53**, 8151 (1996).
[45] E. Z. Kurmaev *et al.*, Phys. Rev. B **57**, 1558 (1998).
[46] We extrapolate the zero-frequency limit (shown in Figs. 2 and 3) from the values of the self-energy at the first Matsubara frequency and by analytical continuation of the self-energy; the two approaches yield similar results.
[47] See Supplemental Material at http://link.aps.org/supplemental/10.1103/PhysRevLett.116.106402 for the $(U, J) = (2.3, 0.4)$ eV Fermi-surface and the frequency dependence of $\Delta\varepsilon_{\rm CF}$.
[48] The spread $\langle|\boldsymbol{r}^2|\rangle$ is 3.79 Å^2 for the xz and 3.55 Å^2 for the xy orbital.
[49] The effect of $\Delta U'$, which modifies interorbital Coulomb terms, is weaker than that of the intraorbital correction ΔU, hence the results of the two sets of calculations are similar. Thus, only results for $\Delta U' = \Delta U/3$ are shown.
[50] For $(U, J) = (2.3, 0.4)$ eV the changes with respect to calculations with isotropic U are smaller.
[51] For isotropic Coulomb interaction, $H_{\rm dc}$ is a mere shift of the chemical potential and has no effect on the parameters.

Instead, for finite ΔU, $H_{dc} \propto \Delta U$. A positive (negative) δH_{dc} yields correspondingly a positive (negative) $\delta\Delta\varepsilon_{CF}$; the other parameters are little affected by δH_{dc}. For realistic δH_{dc} the change $\delta\Delta\varepsilon_{CF}$ is, however, small; an increase of H_{dc} of, e.g., 9%, yields for $\Delta U = 3\Delta U' = 0.45$ eV a $\Delta\varepsilon_{CF} \sim -57$ meV (instead of -83 meV). Thus, the main effect of a $\delta H_{dc} \sim \pm 9\% H_{dc}$ is equivalent to that of a shift of a few tenths of meV on the right or left (depending on the sign of δH_{dc}) of the value of ΔU for which the best agreement with experiments is reached. For comparison, $|\delta H_{dc}| \sim 12\% H_{dc}$ is the difference between the around-mean-field limit and the fully localized limit with $n_{xy} = 1, n_{xz} + n_{yz} = 3$. Hence, our conclusions remain unaffected by δH_{dc} unless H_{dc} becomes unrealistically large, yielding a large orbital polarization, to the best of our knowledge never reported experimentally.

[52] This, together with the Luttinger theorem, allows the $T \to 0$ extrapolation. The strongest temperature dependence is perhaps shown by $\Delta\delta_\lambda$.

[53] For the CF, model calculations [21] yield a similar conclusion. For the SO couplings, a dynamical $\Delta\delta_\lambda$ has been obtained for the hybridization function of insulating Sr iridates, see H. Zhang, K. Haule, and D. Vanderbilt, Phys. Rev. Lett. **111**, 246402 (2013).

[54] Thus, neither the SO interaction nor the crystal field splitting dominate in determining the most occupied states.

[55] In line with our LDA + SO + DMFT results, we assume that also for the model calculations the system is a Fermi liquid satisfying the Luttinger theorem.

[56] The agreement remains good provided that $\Delta\varepsilon_{CF}$ is at least 100 meV smaller than the value obtained with isotropic U and that the SO couplings are correspondingly sufficiently enhanced by Coulomb repulsion. It starts to visibly deteriorate for, e.g., $\Delta\varepsilon_{CF} \sim +0.03$ eV.

[57] T. Scaffidi, J. C. Romers, and S. H. Simon, Phys. Rev. B **89**, 220510(R) (2014).